KdgF, the missing link in the microbial metabolism of uronate sugars from pectin and alginate

Joanne K. Hobbs[a], Seunghyae M. Lee[a], Melissa Robb[a], Fraser Hof[b], Christopher Barr[b], Kento T. Abe[a], Jan-Hendrik Hehemann[a,c,d], Richard McLean[e], D. Wade Abbott[e], and Alisdair B. Boraston[a,1]

[a]Department of Biochemistry and Microbiology, University of Victoria, Victoria, BC, V8W 3P6, Canada; [b]Department of Chemistry, University of Victoria, Victoria, BC, V8W 3P6, Canada; [c]MARUM MPG Bridge Group Marine Glycobiology, Center for Marine Environmental Sciences, University of Bremen, 28334 Bremen, Germany; [d]Max Planck Institute for Marine Microbiology, 28359 Bremen, Germany; and [e]Lethbridge Research Centre, Agriculture and Agri-Food Canada, Lethbridge, AB, T1J 4B1, Canada

Edited by Dan S. Tawfik, The Weizmann Institute of Science, Rehovot, Israel, and accepted by the Editorial Board April 15, 2016 (received for review December 8, 2015)

Uronates are charged sugars that form the basis of two abundant sources of biomass—pectin and alginate—found in the cell walls of terrestrial plants and marine algae, respectively. These polysaccharides represent an important source of carbon to those organisms with the machinery to degrade them. The microbial pathways of pectin and alginate metabolism are well studied and essentially parallel; in both cases, unsaturated monouronates are produced and processed into the key metabolite 2-keto-3-deoxygluconate (KDG). The enzymes required to catalyze each step have been identified within pectinolytic and alginolytic microbes; yet the function of a small ORF, *kdgF*, which cooccurs with the genes for these enzymes, is unknown. Here we show that KdgF catalyzes the conversion of pectin- and alginate-derived 4,5-unsaturated monouronates to linear ketonized forms, a step in uronate metabolism that was previously thought to occur spontaneously. Using enzyme assays, NMR, mutagenesis, and deletion of *kdgF*, we show that KdgF proteins from both pectinolytic and alginolytic bacteria catalyze the ketonization of unsaturated monouronates and contribute to efficient production of KDG. We also report the X-ray crystal structures of two KdgF proteins and propose a mechanism for catalysis. The discovery of the function of KdgF fills a 50-y-old gap in the knowledge of uronate metabolism. Our findings have implications not only for the understanding of an important metabolic pathway, but also the role of pectinolysis in plant-pathogen virulence and the growing interest in the use of pectin and alginate as feedstocks for biofuel production.

uronate | ring opening | tautomerization | pectin | alginate

Polysaccharides, such as those found as biomass in marine algae and terrestrial plants, comprise a vast sink of photosynthetically fixed carbon and a potentially enormous source of energy to organisms with the appropriate metabolic systems to unlock it. Pectin, a complex polyuronate largely made up of the uronate D-galacturonate connected by α-(1,4) linkages, is one such polysaccharide. The principal reservoir of pectin is the primary cell wall of terrestrial plants and, as such, its degradation and metabolism by microbes is an important component of the natural turnover of biomass, infection by plant pathogens, digestion of dietary fiber in the mammalian gut, and the utilization of biomass as feedstocks for biofuels or other valuable products (1). Similarly, alginate, another polyuronate that comprises β-linked D-mannuronate and L-guluronate (in varying lengths and arrangements), is a major cell wall component of brown macroalgae (seaweed). Alginate can comprise up to 40% of the dry weight of the algae, making the recycling of this photosynthetically fixed carbon a significant aspect of the ocean carbon cycle. The prevalence of both polysaccharides in biomass has made them important considerations in the production of ethanol from marine algae and terrestrial plant feedstocks (e.g., refs. 2–4).

The microbial pathways responsible for the metabolism of pectin and alginate are considered well understood and essentially parallel, with both resulting in the production of the key metabolite 2-keto-3-deoxygluconate (KDG) (Fig. 1). For both polysaccharides, the typical process is initiated by endoacting polysaccharide lyases (PLs), which cleave the polysaccharide backbone using a β-elimination mechanism, thus producing oligouronates with 4,5-unsaturated nonreducing ends. After being imported into the microbe, these products are completely degraded to 4,5-unsaturated monouronates by oligouronate-specific PLs (1). In pectinolytic organisms, the conversion of 4,5-unsaturated galacturonate (ΔGalUA) to KDG occurs via three steps and the two intermediates 5-keto-4-deoxyuronate (DKI) and 2,5-diketo-3-deoxygluconate (DKII). The final two steps are catalyzed by an isomerase (KduI) and a reductase (KduD) (5). In alginolytic organisms, 4,5-unsaturated mannuronate (ΔManUA) and guluronate (ΔGulUA) are converted to KDG via two steps and the intermediate 4-deoxy-L-erythro-5-hexoseulose uronate (DEH), with the second step catalyzed by DEH reductase (4) (Fig. 1). The two pathways converge at KDG, which in turn is processed into pyruvate and 3-phosphoglyceraldehyde via the Entner–Doudoroff pathway, ultimately providing energy in a form an organism can readily use.

On the basis of these well-defined metabolic pathways, genes encoding the hallmark enzymes of pectinolytic and alginolytic pathways can be easily identified in a large number of microbial genomes. A general comparison of these predicted enzymes, which are often encoded at a single distinct genomic locus, reveals the consistent cooccurrence and colocalization of a small

Significance

Pectin and alginate are polysaccharides found in the cell walls of plants and brown algae, respectively. These polysaccharides largely consist of chains of uronates, which can be metabolized by bacteria through a pathway of enzymatic steps to the key metabolite 2-keto-3-deoxygluconate (KDG). Understanding the metabolism of these sugars is important because pectin degradation is used by many plant-pathogenic bacteria during infection, and both pectin and alginate represent abundant sources of carbohydrate for the production of biofuels. Here we demonstrate that KdgF, a protein of previously unknown function, catalyzes the linearization of unsaturated uronates from both pectin and alginate. Furthermore, we show that KdgF contributes to efficient production of KDG and a bacterium's ability to grow on uronates.

Author contributions: J.K.H. and A.B.B. designed research; J.K.H., S.M.L., M.R., C.B., K.T.A., J.-H.H., R.M., and D.W.A. performed research; J.K.H., F.H., and A.B.B. analyzed data; and J.K.H. and A.B.B. wrote the paper.

The authors declare no conflict of interest.

This article is a PNAS Direct Submission. D.S.T. is a guest editor invited by the Editorial Board.

Data deposition: The atomic coordinates and structure factors have been deposited in the Protein Data Bank, www.pdb.org (PDB ID codes 5FPX, 5FPZ, and 5FQ0). The sequences reported in this paper have been deposited in the GenBank database (accession nos. KU156827 and KU697803–KU697810).

[1]To whom correspondence should be addressed. Email: boraston@uvic.ca.

This article contains supporting information online at www.pnas.org/lookup/suppl/doi:10.1073/pnas.1524214113/-/DCSupplemental.

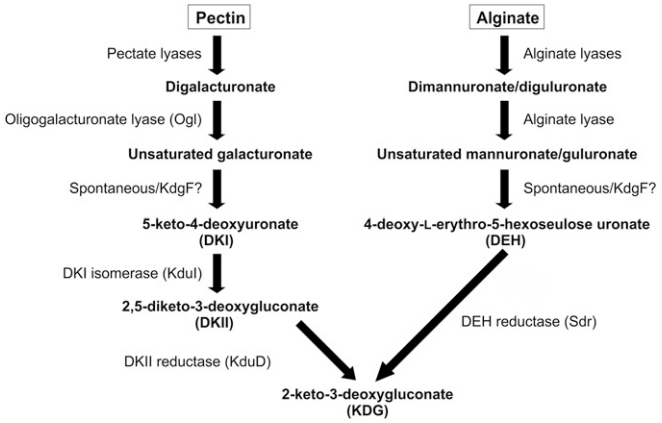

Fig. 1. Schematic depiction of the major steps in the degradation of unsaturated uronates from pectin and alginate.

ORF called *kdgF* in both pectinolytic and alginolytic systems (*SI Appendix*, Fig. S1) (6). *kdgF* was initially identified within the pectin degradation locus of *Dickeya dadantii* (formerly *Erwinia chrysanthemi*) where it was observed to be regulated by the pectin degradation repressor protein KdgR (5). Although disruption of *kdgF* in *D. dadantii* did not prevent growth on polygalacturonate (PGA), it did result in lower induction of pectate lyases by PGA and reduced maceration of potato tubers. Thus, KdgF is now annotated as a cupin-like protein involved in pectin degradation (InterPro IPR025499). The specific role of KdgF in pectin metabolism has not been uncovered, nor has the reason for the occurrence of KdgF homologs in alginate-processing loci been addressed.

Examination of the pectin and alginate metabolism pathways reveals that a known enzyme catalyzes each step, with the exception of the conversion of ΔGalUA and ΔManUA/ΔGulUA into DKI and DEH, respectively (Fig. 1). The initial conversion of the 4,5-unsaturated monouronates is assumed to occur spontaneously and proceed by opening of the pyranose ring followed by an enol–keto tautomerization (4, 7–9). The timescales of monosaccharide mutarotation (which include a ring opening) and known enol–keto tautomerizations are on the order of minutes to hours (10–12), making the likely timescale of the proposed spontaneous conversion of 4,5-unsaturated monouronates too large to be feasibly incorporated into an efficient metabolic pathway. Given that KdgF is the only conserved component of pectinolytic and alginolytic pathways without a known function, we hypothesized that this protein in fact catalyzes the generation of DKI or DEH. In this study, we use a combination of enzyme activity assays, X-ray crystallography, mutagenesis, and NMR to demonstrate that KdgF from both pectinolytic and alginolytic loci catalyzes the initial conversion step of 4,5-unsaturated monouronates. Furthermore, we show that KdgF from a pectinolytic system contributes to efficient production of KDG in a reconstituted in vitro pathway and in the context of microbial growth on PGA in vivo.

Results

KdgF Catalyzes Double Bond Depletion in Unsaturated Monouronates. For this study, we initially focused on the pectinolytic locus from *Yersinia enterocolitica* (*SI Appendix*, Fig. S1), which is one of the most thoroughly structurally and functionally characterized pectinolytic systems, with only the function of the KdgF component (*Ye*KdgF) being unknown (e.g., refs. 1, 13, and 14). As the predicted substrate of KdgF spontaneously converts at a significant rate, we could not assay the activity of recombinant *Ye*KdgF on ΔGalUA directly. Instead, a linked assay was used where the oligogalacturonate lyase from *Y. enterocolitica* (*Ye*Ogl) was incubated with digalacturonate [α-D-GalUA-(1–4)-D-GalUA] to produce 1 mole of ΔGalUA per mole of digalacturonate (*SI Appendix*, Fig. S2). The formation of ΔGalUA by *Ye*Ogl can be monitored by absorbance of the newly formed 4,5-double bond of the enol product at 230 nm (13). Thus, we reasoned that the predicted production of the linearized ketone tautomer of the monosaccharide by *Ye*KdgF could be monitored by a decrease in the absorbance after addition of the protein. Indeed, the addition of *Ye*KdgF to the samples after the *Ye*Ogl reactions had reached equilibrium (judged by a stable absorbance reading) resulted in a rapid decrease in the A_{230nm} in a manner that was dependent upon the concentration of *Ye*KdgF and, therefore, consistent with the catalyzed depletion of the double bond in ΔGalUA (Fig. 2*A*). In the presence of 200 nM *Ye*KdgF, the catalyzed rate of double bond depletion was ∼30-fold greater than the fastest spontaneous rate observed.

To assess the activity of KdgF on ΔManUA, we performed a parallel experiment using dimannuronate [β-D-ManUA-(1–4)-D-ManUA], the oligoalginate lyase Alg17c from *Saccharophagus degradans* (15) to produce ΔManUA and *Ha*KdgF from the alginate processing locus of a *Halomonas* sp. isolated from brown algae (*SI Appendix*, *SI Methods*). *Ha*KdgF also catalyzed double bond depletion in a concentration-dependent manner; however, slightly higher concentrations of enzyme were required (Fig. 2*B*).

Thus, *Ye*KdgF and *Ha*KdgF are both able to convert the products of their respective upstream enzymes. These enzymes share >50% amino acid sequence identity, whereas ΔGalUA and ΔManUA differ only by being C2 epimers, suggesting that the enzymes may be cross-specific. Therefore, we tested the activity of *Ye*KdgF and *Ha*KdgF on the products of Alg17c and *Ye*Ogl, respectively, which represent their nonnatural substrates. Both enzymes were able to catalyze double bond depletion in their alternative substrate and have roughly equivalent abilities to do so (*SI Appendix*, Fig. S3). Due to the nature of the lyase-coupled assay, we were unable to determine Michaelis–Menten parameters for the different enzyme–substrate combinations; however, comparison of initial velocities estimated from curves generated under the same experimental conditions suggest that the enzymes have similar activities on each of the substrates and both have a more than threefold preference for ΔGalUA over ΔManUA (*SI Appendix*, Table S1).

***Ye*KdgF Catalyzes the Conversion of ΔGalUA to DKI.** The results of our enzyme assay are consistent with *Ye*KdgF and *Ha*KdgF catalyzing double bond depletion within unsaturated monouronates, which we presume to be a result of the enol–ketone tautomerization that occurs after ring opening. In the case of ΔGalUA, the reported product of this conversion step, and therefore the expected product of *Ye*KdgF, is DKI (Fig. 1). To provide support for this, we used NMR to compare the products of spontaneous conversion of ΔGalUA and the *Ye*KdgF catalyzed reaction (Fig. 3). For this experiment, we used 4,5-unsaturated digalacturonate ($\Delta GalUA_2$), as cleavage of this disaccharide by *Ye*Ogl produces two molecules of ΔGalUA. An overlay of the 1D selective total correlation spectroscopy (TOCSY) NMR subspectra for $\Delta GalUA_2$ treated with *Ye*Ogl and *Ye*KdgF, or *Ye*Ogl alone, reveals that both reactions produce the same two isomeric products (Fig. 3*A*). From their resonances, coupling

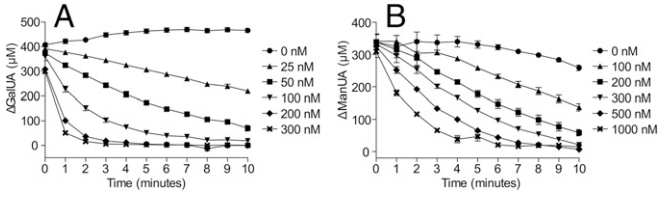

Fig. 2. Activity of *Ye*KdgF and *Ha*KdgF on unsaturated uronates. Double bond depletion in unsaturated monouronates in the presence of *Ye*KdgF or *Ha*KdgF was followed at 230 nm using a lyase-coupled assay (*SI Appendix*, Fig. S2). (*A*) Concentration-dependent activity of *Ye*KdgF on ΔGalUA. (*B*) Concentration-dependent activity of *Ha*KdgF on ΔManUA. Error bars, where visible, represent the SEM (n = 3).

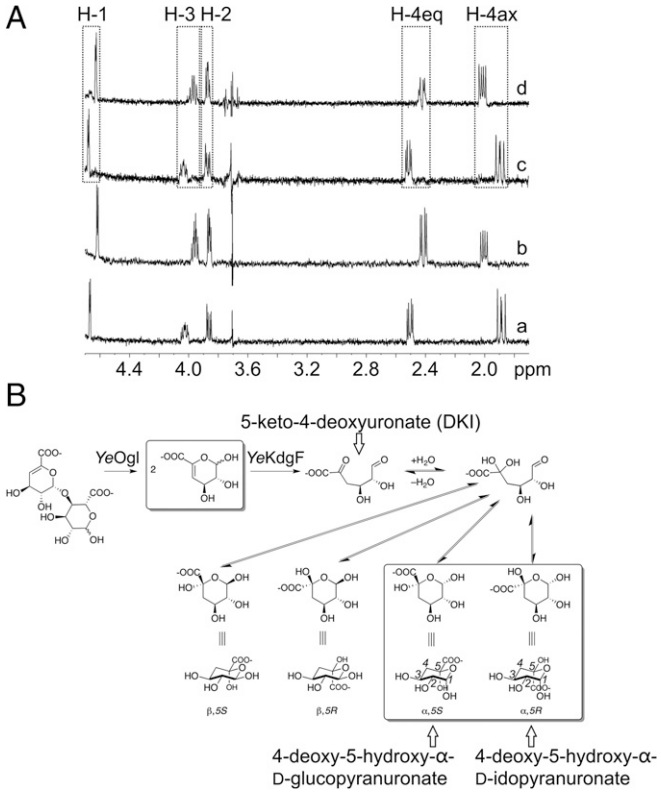

Fig. 3. One-dimensional selective TOCSY NMR determination of the product of *Ye*KdgF. (*A*) One-dimensional selective TOCSY NMR subspectra of the products produced from $\Delta GalUA_2$ by the action of either *Ye*Ogl and *Ye*KdgF (*a* and *b*) or *Ye*Ogl alone (*c* and *d*). In both cases, two products were observed: 4-deoxy-5-hydroxy-α-D-idopyranuronate (*a* and *c*) and 4-deoxy-5-hydroxy-α-D-glucopyranuronate (*b* and *d*). Coupling constants for the two observed products and detailed explanation of structural assignments are given in *SI Appendix*. Dashed boxes indicate the peaks for H-1, H-2, H-3, H-4 axial, and H-4 equatorial, which correspond to the carbon numbering shown on the two observed products in *B*. (*B*) Proposed reaction scheme for the action of *Ye*Ogl and *Ye*KdgF upon $\Delta GalUA_2$ under NMR observation. The spontaneous and *Ye*KdgF-catalyzed ring opening is followed by two rapid steps: hydration of the electron-poor keto-acid carbonyl and ring closure to form the two pyranose α-anomers shown. No evidence for β-anomeric products is present. The boxed species are observed directly by NMR.

patterns and chemical shifts, we identified these two final products as isomers of a pyranose, closed-ring form of DKI (Fig. 3*B* and *SI Appendix*). We propose that formation of pyranose rings occurs after spontaneous hydration of the electron-poor ketone carbonyl before cyclization of the hydrate onto the aldehyde. Two of the four possible diastereomers are formed (Fig. 3*B*). The small C1(H)–C2(H) coupling constant of 3.7 Hz in both products indicates that they are both α-anomers; no β-anomeric resonances were seen (16). All chemical shifts and coupling constants (*SI Appendix*, Tables S2 and S3) are consistent with the products being 4-deoxy-5-hydroxy-α-D-glucopyranuronate and 4-deoxy-5-hydroxy-α-D-idopyranuronate.

KdgF Is Important to KDG Production and Growth on Polygalacturonate. Our data are consistent with the production of DKI by *Ye*KdgF from the product of *Ye*Ogl catalysis. In the *Y. enterocolitica* system, the *Ye*KdgF-catalyzed generation of DKI would provide the substrate for downstream processing by the isomerase *Ye*KduI and the NADH-dependent reductase *Ye*KduD into KDG (5). To test this, we established a coupled assay in which the oxidation of NADH by *Ye*KduD is linked to the sequential processing of digalacturonate by *Ye*Ogl, *Ye*KdgF, and *Ye*KduI (Fig. 4*A*). When all four enzymes were present, we observed time-dependent turnover of NADH. The omission of *Ye*KdgF resulted in a significant decrease in NADH turnover at each time point ($P = 0.0201$, paired t test, $n = 3$) of 57–69%. In comparison, omission of either *Ye*Ogl, *Ye*KduI, or *Ye*KduD resulted in an 81–93% decrease in NADH turnover. The oxidation of NADH in the absence of KdgF is consistent with the spontaneous production of DKI, whereas the dramatic increase of NADH turnover in the presence of *Ye*KdgF reveals the important role of this protein in generating DKI and increasing flux through the reconstituted pathway.

The positive effect of *Ye*KdgF on the rate of KDG production suggests that KdgF would contribute toward efficient pectin catabolism in vivo. Most strains of *Escherichia coli* cannot grow on PGA as the sole carbon source as they contain only a subset of the uronate utilization genes found in *Y. enterocolitica* (6). However, some strains, including American Type Culture Collection (ATCC) 25922, contain an additional uronate utilization locus, which includes *kdgF* (*SI Appendix*, Fig. S1). We produced KdgF from ATCC 25922 (*Ec*KdgF) recombinantly and confirmed that it catalyzes conversion of ΔGalUA in vitro (*SI Appendix*, Fig. S4). We then tested the ability of ATCC 25922 to grow on PGA and found that it could do so if the medium was supplemented with the endoacting polygalacturonate lyase *Ye*PL2A (14) to promote generation of oligogalacturonides (examination of the genome of ATCC 25922 reveals that it lacks its own endoacting PL). A markerless *kdgF* deletion mutant of ATCC 25922 displayed a >40% reduction in growth rate on *Ye*PL2A-treated PGA compared with wild-type ATCC 25922 and complemented strains (Fig. 4*B*; $0.49 \cdot h^{-1}$ for wild type vs. $0.28 \cdot h^{-1}$ for Δ*kdgF*, $P \leq 0.001$, one-way ANOVA with Tukey's test). There was no statistically significant difference in lag time between the strains under these conditions ($P > 0.05$, one-way ANOVA with Tukey's test). This decrease in growth rate is consistent with our in vitro coupled enzyme data where in the absence of KdgF, KDG production was not completely abolished but was decreased to a basal level of spontaneous ΔGalUA conversion.

X-Ray Crystallographic Analysis of KdgF. To provide insight into the molecular details behind the activity of KdgF, we determined the X-ray crystal structures of *Ye*KdgF and *Ha*KdgF. The initial crystal form of *Ye*KdgF in the spacegroup $P2_12_12_1$ yielded diffraction data to 1.5-Å resolution and the structure was solved by molecular replacement to give a model with two molecules of the protein in the asymmetric unit. Each *Ye*KdgF monomer adopts the canonical β-barrel cupin fold (Fig. 5*A*). The two molecules of *Ye*KdgF modeled in the asymmetric unit were related by C2 noncrystallographic symmetry (Fig. 5*A*) and, as determined by PISA (Proteins, Interfaces, Structures and Assemblies) analysis,

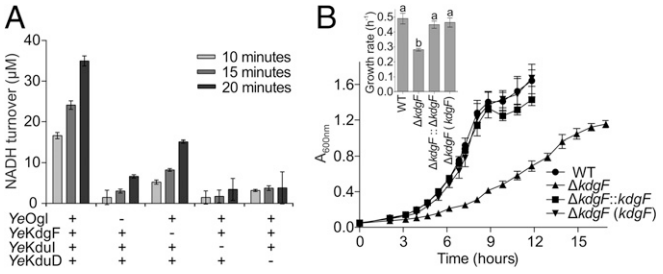

Fig. 4. KdgF contributes to KDG production and growth on polygalcturonate. (*A*) Linked assay in which the production of KDG (and concomitant oxidation of NADH) is dependent on the sequential processing of digalacturonate by *Ye*Ogl, *Ye*KdgF, *Ye*KduI, and *Ye*KduD. Data shown indicate the effect of omitting one of the four enzymes. Error bars represent the SEM ($n = 3$). (*B*) Δ*kdgF* mutant of *E. coli* ATCC 25922 displays a reduced growth rate on PGA compared with wild-type and complemented strains (either *kdgF* reinserted into the genome or provided on a plasmid). Error bars represent the SEM ($n = 4$). The *Inset* bar chart indicates the mean growth rate determined for each strain from the growth curves shown. Lowercase letters above bars indicate statistically significant differences between means as determined by a one-way ANOVA with Tukey's test ($P \leq 0.01$).

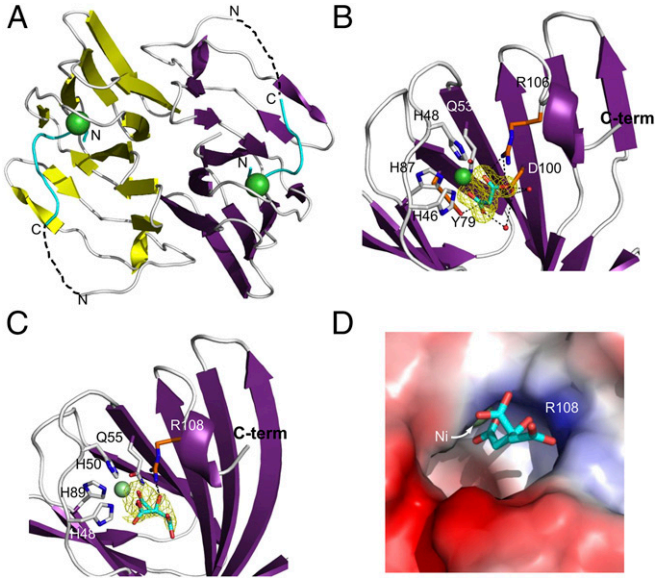

Fig. 5. X-ray crystal structures of *Ye*KdgF and *Ha*KdgF. (*A*) Cartoon representation of the *Ye*KdgF dimer (PDB 5FPX). Dashed lines approximate what is a likely disordered and therefore unmodeled region. (*B*) Structure of *Ye*KdgF in spacegroup $P3_221$ showing the ordered C terminus and bound malonate molecule (PDB 5FPZ). (*C*) Structure of *Ha*KdgF with a citrate molecule adjacent to the metal atom (PDB 5FQ0). In *B* and *C* the bound ligands (light blue sticks) and their F_o–F_c electron density maps (contoured at 3σ; yellow mesh) are shown. Residues coordinating the bound metal atom (gray sticks) and interacting with the bound ligands (orange sticks) are shown. (*D*) The solvent accessible surface of the KdgF metal binding site, as represented by *Ha*KdgF in complex with citrate. In *A*–*D*, a bound metal that was modeled as a Ni^{2+} atom is shown (green sphere).

associated via an extensive surface comprising 1689 $Å^2$ of interface area, 14 hydrogen bonds, six salt bridges, and a predicted binding energy of −30 kcal/mole, indicating this is the biological assembly for *Ye*KdgF.

The active site of each monomer contained a metal atom coordinated by three histidines and a glutamine. Analysis of *Ye*KdgF crystals by X-ray fluorescence excitation yielded emission peaks at 7.5 keV and 8.3 keV, which match most closely the KL and KM edges of Ni (*SI Appendix*, Fig. S5*A*). A multiwavelength anomalous dispersion (MAD) scan of the crystals at the nickel edge revealed anomalous scattering from nickel, and anomalous difference maps from data collected at the peak wavelength for anomalous scattering by this metal localized the anomalous signal to the metal atom associated with the protein (*SI Appendix*, Fig. S5 *B* and *C*). Furthermore, the refined coordination bond geometry and distances were consistent with Ni^{2+}, as was the refined B factor when the atom was modeled as a Ni^{2+}.

The N terminus of a sequence corresponding to the six-histidine tag used for purification of *Ye*KdgF was found associated with the metal atom (*SI Appendix*, Fig. S6), likely resulting in the C-terminal sequence of KRDDFL being disordered. We explored an alternate crystal form obtained in the spacegroup $P3_221$, which contained a single monomer in the asymmetric unit; a dimer generated by the crystallographic twofold axis was the same as that observed in the $P2_12_12_1$ crystal form. This structure revealed an ordered and complete C terminus that flanks the metal binding site (Fig. 5*B*). Electron density for a malonate molecule derived from the tacsimate in the crystallization condition was found adjacent to the metal atom. The modeled malonate was bound by the metal atom, R106, and water mediated interactions with Y79 and D100 (Fig. 5*B*).

We also solved the structure of *Ha*KdgF to 2.35-Å resolution. The protein crystallized with two dimers of *Ha*KdgF in the asymmetric unit, with each dimer having a root mean square deviation of 0.5 Å with the *Ye*KdgF dimer over all of the Cαs (*SI Appendix*, Fig. S7). Electron density consistent with a citrate molecule derived from the crystallization condition was found adjacent to the metal atom in each of the monomers (Fig. 5*C*). Unlike the malonate in *Ye*KdgF, where each of the carboxylate groups interacted with the metal atom, only a single carboxylate of the citrate in *Ha*KdgF was coordinated by the metal. R108 made a hydrogen bond with the central hydroxyl group of the citrate (Fig. 5*C*).

For both *Ye*KdgF and *Ha*KdgF, the metal binding sites sit at the bottom and to the side of a distinct pocket in the surface of the protein, with the malonate and citrate molecules accommodated in the pocket (Fig. 5*D*). The dimensions of the opening to the pocket are ∼10 Å × 10 Å, whereas it has a maximum depth of ∼12 Å, and thus of roughly sufficient size to accommodate binding of either a closed ring uronate (∼6-Å maximum dimension) or open ring uronate (∼8-Å maximum dimension).

Identification of the KdgF Active Site. The amino acid residues lining the pocket housing the metal binding site in *Ye*KdgF are highly conserved with *Ha*KdgF (Fig. 6*A*) and indeed the KdgF family (*SI Appendix*, Fig. S8). Thus, this pocket of the protein is an obvious candidate for the active site. To probe the role of the metal in catalysis, *Ye*KdgF was depleted of metal and then reconstituted by the addition of exogenous metals and assayed. The enzyme proved to be inactive when metal depleted, whereas several metals, including Ni^{2+}, were able to restore activity to levels higher than the untreated enzyme (Fig. 6*B*). This points to the importance of the metal in the activity of *Ye*KdgF, whereas the greater activity of the reconstituted enzymes suggests that the untreated enzyme may have had only partial occupation of the metal binding site. Due to the presence of Ni^{2+} during the

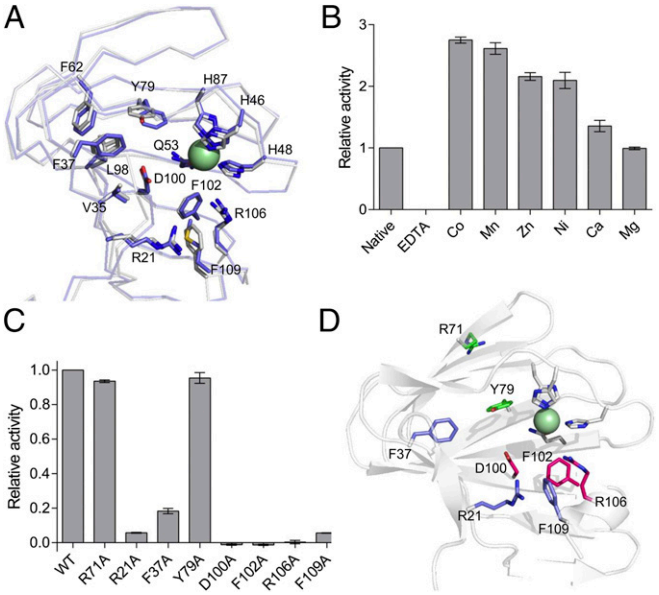

Fig. 6. Metal dependence of *Ye*KdgF and identification of the active site. (*A*) Overlay of *Ye*KdgF and *Ha*KdgF structures showing the conserved residues that line the proposed active site pocket. Residue numbering corresponds to *Ye*KdgF. (*B*) Metal dependence of *Ye*KdgF activity. *Ye*KdgF was treated with EDTA and then dialyzed against buffer containing different metals (or no metal). Initial rate of activity is shown relative to native *Ye*KdgF. (*C*) Catalytic activity of alanine mutants of *Ye*kdgF. A number of residues that line the proposed active site pocket were mutated to alanine and the mutant proteins assayed for activity. Initial rate of activity is shown relative to wild type. In *B* and *C*, error bars represent the SEM ($n = 4$). (*D*) Positons of mutated residues shown on the *Ye*KdgF structure and color coded according to the effect of the alanine substitution on activity: magenta, no activity; light purple, reduced activity; and green, no effect on activity.

BIOCHEMISTRY

immobilized metal affinity chromatography purification of *Ye*KdgF, we are unable to say whether Ni^{2+} is the biological metal, although it is clear the enzyme can function when bound to several different metal ions.

We continued analysis of the active site by making alanine substitution mutants of seven residues in *Ye*KdgF that are conserved with *Ha*KdgF and project into the putative active site cleft. An R71A mutation was included as a control, as its position in the structure of *Ye*KdgF would not be expected to affect activity. Of the seven proposed active site mutants, three of them (D100A, F102A, and R106A) displayed no catalysis of double bond depletion (Fig. 6 *C* and *D*); reactions were allowed to proceed for at least 30 min but still showed no activity above background (*SI Appendix*, Fig. S9). Three further mutants (R21A, F37A, and F109A) exhibited reduced activity, whereas the R71A and Y79A mutants displayed activity comparable with wild type (Fig. 6 *C* and *D*). All mutant proteins were confirmed to be folded using differential scanning fluorimetry (*SI Appendix*, Fig. S10). Taken in concert with the metal depletion data, this supports the identification of the cleft housing the metal binding site as the active site of *Ye*KdgF and likely all KdgF proteins.

Discussion

The steps for the enzymatic conversion of ΔManUA acid to KDG were delineated by a series of elegant experiments over 50 y ago (8, 17). Subsequently, these steps have been found to be largely paralleled in the enzymatic conversion of ΔGalUA acid to KDG (9, 18). However, the assumption has been that bacteria rely on spontaneous conversion of the 4,5-unsaturated monouronate to DKI or DEH (4, 8, 9); yet this does not seem to be the case. In vitro, both *Ye*KdgF and *Ha*KdgF were able to deplete the 4,5-unsaturated monouronate products of oligouronate lyase reactions, and the reaction products generated by *Ye*KdgF were determined to have NMR properties consistent with DKI. Including *Ye*KdgF in a reconstituted pathway increased the activity of the final enzyme in the pathway, KduD, which generates KDG, revealing the ability of *Ye*KdgF to produce the DKI substrate of KduI and its overall importance to the efficiency of the pathway. Finally, KdgF contributed to the in vivo capacity of an *E. coli* strain to grow on enzymatically fragmented polygalacturonate. Thus, the results of our experiments support the conclusion that *Ye*KdgF and *Ha*KdgF, components of pectinolytic and alginolytic pathways, respectively, catalyze the ketonization of 4,5-unsaturated uronates, thereby filling an over 50-y-old gap in the knowledge of these metabolic pathways.

Although the pathways of depolymerizing pectins and alginate to 4,5-unsaturated uronates are procedurally parallel, microbes must deploy multiple enzymes belonging to different carbohydrate-active enzyme families to depolymerize the two different polysaccharides (Fig. 1); interestingly, KdgF is the only component conserved between the pectin and alginate utilization pathways. Bioinformatic analysis of KdgF reveals that it is most prevalent among members of the Proteobacteria, to which *Y. enterocolitica* and *Halomonas* sp. belong. However, KdgF homologs are also widely dispersed among other, diverse phyla of bacteria (such as Bacteroidetes, Spirochaetes, and Firmicutes) and some Archaea. The composition and arrangement of pectin and alginate utilization loci can vary greatly between organisms, but *kdgF* is typically associated with a hallmark enzyme, such as a PL or a KDG-processing enzyme (*SI Appendix*, Fig. S11). The perpetual occurrence of *kdgF* in pectinolytic and alginolytic prokaryotes (despite the variety in genomic context), its wide distribution among different phyla of Bacteria and Archaea, and its position as the only conserved component between the pectin and alginate utilization pathways underlines its importance in efficient metabolism of uronates. Intriguingly, there are a small number of organisms, such as the cyanobacterium *Chroococcidiopsis thermalis* and the archaeon *Pyrobaculum aerophilum*, whose genomes encode for a predicted KdgF but no known PLs or other enzymes associated with uronate metabolism [according to the Kyoto Encyclopedia of Genes and Genomes (KEGG) database] (19), leaving their putative functions unclear.

The conversion of 4,5-unsaturated uronates to the ketonized linear form requires an opening of the ring and an enol–keto tautomerization. Given that the spontaneous opening of pyranose rings occurs on the order of minutes, whereas some enol–keto tautomerizations happen on an analogous timescale, it is possible that KdgF catalyzes both the ring opening and the enol–keto tautomerization (10–12). Catalyzed pyranose ring-opening reactions, as exemplified by galactose mutarotase, occur through protonation of the endocyclic O5 and deprotonation of the C1 hydroxyl group by separate amino acid sidechains acting as acid and base catalysts, respectively (20). Thus, by analogy, we propose that KdgF catalyzes a similar ring opening to generate the linear enol form of the 4,5-unsaturated uronates (Fig. 7*A*). Likewise, we anticipate the potential enol–keto tautomerization catalyzed by KdgF to be similar to that performed by macrophage migration inhibitory factor on phenylpyruvate (21). In our proposed ketonization reaction, the newly formed O5 enol hydroxyl of the linearized sugar would be deprotonated followed by protonation of C4 to generate the final ketone product (Fig. 7*A*). In this reaction, the role of the divalent metal is most likely to coordinate the substrate carboxylate, thereby stabilizing the interaction and orienting the substrate. The ability of the metal to neutralize the charge of the substrate carboxylate may also play a role in catalysis.

Some support for the proposed reaction scheme is provided by our structural and mutagenesis studies. Mutagenesis of F102, D100, and R106 revealed these amino acids to be indispensable for the catalytic activity of *Ye*KdgF, with the sidechains of the latter two residues having chemical properties consistent with the ability to act as a general acid and/or base. To approximate the possible initial binding mode of ΔGalUA, we structurally overlapped *Ye*KdgF with *Ha*KdgF and then overlapped the carboxylic acid of ΔGalUA with the metal-bound carboxylic acid of the *Ha*KdgF-bound citrate molecule (Fig. 7*B*). From this we find that O5 and C4 of ΔGalUA come in proximity (within 3–4 Å) to R106 and D100, respectively, in *Ye*KdgF (R108 and D102 in *Ha*KdgF; Fig. 7*B*). The alternate orientation of ΔGalUA (i.e., the pyranose ring rotated 180° around the C5–C6 bond) brings O5 and C4 of ΔGalUA in proximity to D100 and R106, respectively. Thus, consistent with their general importance to the catalytic activity of KdgF, the sidechains of these residues may be appropriately positioned relative to key atoms in the substrate to perform as acid and/or base catalysts. However, further work is necessary to detail the participation of these sidechains in the molecular basis of KdgF catalysis. Notably, our proposed mode of uronate binding focuses recognition and catalytic reactions on

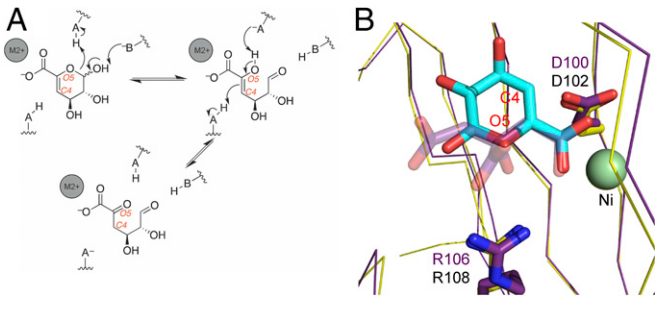

Fig. 7. Proposed catalytic mechanism of KdgF. (*A*) Schematic depiction of the two proposed reactions catalyzed by KdgF. The first step is a ring opening, the second an enol–keto tautomerization. Hypothetical acid/base catalysts that would be present on the enzyme are indicated. Gray spheres represent the divalent metal. (*B*) Overlay of *Ye*KdgF (yellow) with the citrate-bound *Ha*KdgF (purple). ΔGalUA (light-blue sticks) was overlapped with the citrate molecule (transparent purple sticks) via its carboxylate and the nickel-coordinated carboxylate of the citrate to approximate a possible binding mode of ΔGalUA. The proposed aspartate and arginine catalytic residues are shown as sticks.

the C4–C5–C6–O5 portion of the substrate, which is planar by virtue of the sp^2-hybridized C5. This conformation would be shared by all 4,5-unsaturated monouronates, perhaps explaining the interchangeable activity of *Ye*KdgF and *Ha*KdgF on the C2 epimers ΔGalUA and ΔManUA and, by extrapolation, giving them postulated activity on the ΔGulUA that also results from alginate depolymerization.

Here we have shown that KdgF is a central component of uronate metabolism and that it contributes to efficient production of the key metabolite KDG from lyase-catalyzed depolymerization of pectin and alginate. Given our ever-increasing demand for energy, and the role that both pectin and alginate have as components of feedstocks for biofuel production, the discovery of the role of KdgF in efficient uronate metabolism has the potential to be quite impactful. A number of studies have focused on the engineering of microbial platforms for efficient ethanol production from alginate but have overlooked the role of KdgF. In a study by Wargacki et al. (4), an alginate utilization locus from *Vibrio splendidus* was integrated into *E. coli* and the importance of individual genes assessed by deletion and growth assays. Due to the unknown function of *kdgF* at that time, the importance of this gene for growth on alginate (and subsequent production of ethanol) was not evaluated. Given the growth defect on PGA that we observed following *kdgF* deletion, we anticipate that a similar phenotype would be observed with growth on alginate upon deletion of *kdgF* from the *V. splendidus* locus. Due to its unknown function, KdgF was also omitted from the engineering of a synthetic yeast platform for ethanol production from brown macroalgae (3); in light of our findings, we would expect its inclusion to increase the efficiency of ethanol production. Finally, our findings explain the decrease in virulence observed upon disruption of *kdgF* in *D. dadantii* more than 20 y ago (5). The purpose and environment of uronate metabolism in microbes can vary—from carbon source utilization to virulence, from terrestrial and marine environments to the mammalian gut—but KdgF appears to be a maintained and central component of this pathway.

Materials and Methods

Genes encoding for KdgFs, *Ye*KduI and *Ye*KduD, were amplified from genomic DNA and cloned into pET28a for expression. All proteins, with the exception of Alg17c (16), were expressed and purified as previously described (22). KdgF enzyme assays were performed with 1 mM digalacturonate or dimannuronate, 0.5 μM *Ye*Ogl or Alg17c, and varying concentrations of KdgF [an equivalent volume of 20 mM Tris·HCl (pH 8.0) was added to the 0-nM KdgF reactions]. Unsaturated uronates were detected at 230 nm and absorbance values converted to micromolar using an extinction coefficient of 5,200 $M^{-1}{\cdot}cm^{-1}$ (7) following subtraction of the blank (initial absorbance of digalacturonate or dimannuronate). Metal dependence was assayed essentially as described by McLean et al. (22). The linked assay contained 1 mM digalacturonate, 200 μM NADH, and 0.5 μM each enzyme. Activity was followed at 340 nm. ^{1}H NMR spectra were recorded on a Bruker AV-500 spectrometer at 500 MHz with a double presaturation to eliminate the water and Tris·HCl resonances. $\Delta GalUA_2$ (1 mM) was digested with 1 μM *Ye*KdgF and/or 1 μM *Ye*Ogl. When the spectra stabilized (indicating that the reactions had reached completion), 1D selective TOCSY subspectra were obtained. Deletion of *kdgF* was performed using the plasmid pKOV-unstuff (23). Complementation was achieved either by reinsertion of *kdgF* at the site of deletion or by providing *kdgF in trans*. The contribution of *kdgF* to growth on PGA was assessed in minimal medium containing 0.4% (wt/vol) PGA and 0.5 μM *Ye*PL2A. *Ye*KdgF and *Ha*KdgF were crystallized by the hanging drop method following optimization of the crystallization condition. All structures were solved by molecular replacement. Data collection and refinement statistics can be found in *SI Appendix*, Table S4. (For additional details, see *SI Appendix, SI Methods*).

ACKNOWLEDGMENTS. We thank Benjamin Kerr and Satish Nair for providing materials and the Genome Sciences Centre of the British Columbia Cancer Agency for performing the genome sequencing reactions and genome assembly. We thank the staff at the Canadian Light Source (CLS) where diffraction data were collected. The CLS is supported by the Natural Sciences and Engineering Research Council of Canada, the National Research Council Canada, the Canadian Institutes of Health Research, the province of Saskatchewan, Western Economic Diversification Canada, and the University of Saskatchewan. This research was supported by Natural Sciences and Engineering Research Council of Canada Discovery Grant FRN 04355. A.B.B. acknowledges the support of an E. W. R. Steacie Memorial Fellowship.

1. Abbott DW, Boraston AB (2008) Structural biology of pectin degradation by Enterobacteriaceae. *Microbiol Mol Biol Rev* 72(2):301–316.
2. Edwards MC, Doran-Peterson J (2012) Pectin-rich biomass as feedstock for fuel ethanol production. *Appl Microbiol Biotechnol* 95(3):565–575.
3. Enquist-Newman M, et al. (2014) Efficient ethanol production from brown macroalgae sugars by a synthetic yeast platform. *Nature* 505(7482):239–243.
4. Wargacki AJ, et al. (2012) An engineered microbial platform for direct biofuel production from brown macroalgae. *Science* 335(6066):308–313.
5. Condemine G, Robert-Baudouy J (1991) Analysis of an *Erwinia chrysanthemi* gene cluster involved in pectin degradation. *Mol Microbiol* 5(9):2191–2202.
6. Rodionov DA, Gelfand MS, Hugouvieux-Cotte-Pattat N (2004) Comparative genomics of the KdgR regulon in *Erwinia chrysanthemi* 3937 and other gamma-proteobacteria. *Microbiology* 150(Pt 11):3571–3590.
7. Shevchik VE, Condemine G, Robert-Baudouy J, Hugouvieux-Cotte-Pattat N (1999) The exopolygalacturonate lyase PelW and the oligogalacturonate lyase Ogl, two cytoplasmic enzymes of pectin catabolism in *Erwinia chrysanthemi* 3937. *J Bacteriol* 181(13):3912–3919.
8. Preiss J, Ashwell G (1962) Alginic acid metabolism in bacteria. I. Enzymatic formation of unsaturated oligosaccharides and 4-deoxy-L-erythro-5-hexoseulose uronic acid. *J Biol Chem* 237:309–316.
9. Preiss J, Ashwell G (1963) Polygalacturonic acid metabolism in bacteria. I. Enzymatic formation of 4-deoxy-L-threo-5-hexoseulose uronic acid. *J Biol Chem* 238:1571–1583.
10. Huang L, et al. (2007) Study on the kinetics of keto-enol tautomerism of p-hydroxyphenylpyruvic acid using capillary electrophoresis. *J Chromatogr A* 1175(2):283–288.
11. Wertz PW, Garver JC, Anderson L (1981) Anatomy of a complex mutarotation. Kinetics of tautomerization of α-D-galactopyranose and β-D-galactopyranose in water. *J Am Chem Soc* 103(13):3916–3922.
12. Zhou CC, Hill DR (2007) The keto-enol tautomerization of ethyl butylryl acetate studied by LC-NMR. *Magn Reson Chem* 45(2):128–132.
13. Abbott DW, Gilbert HJ, Boraston AB (2010) The active site of oligogalacturonate lyase provides unique insights into cytoplasmic oligogalacturonate β-elimination. *J Biol Chem* 285(50):39029–39038.
14. Abbott DW, Boraston AB (2007) A family 2 pectate lyase displays a rare fold and transition metal-assisted β-elimination. *J Biol Chem* 282(48):35328–35336.
15. Park D, Jagtap S, Nair SK (2014) Structure of a PL17 family alginate lyase demonstrates functional similarities among exotype depolymerases. *J Biol Chem* 289(12):8645–8655.
16. Jongkees SA, Withers SG (2011) Glycoside cleavage by a new mechanism in unsaturated glucuronyl hydrolases. *J Am Chem Soc* 133(48):19334–19337.
17. Preiss J, Ashwell G (1962) Alginic acid metabolism in bacteria. II. The enzymatic reduction of 4-deoxy-L-erythro-5-hexoseulose uronic acid to 2-keto-3-deoxy-D-gluconic acid. *J Biol Chem* 237:317–321.
18. Preiss J, Ashwell G (1963) Polygalacturonic acid metabolism in bacteria. II. Formation and metabolism of 3-deoxy-D-glycero-2, 5-hexodiulosonic acid. *J Biol Chem* 238:1577–1583.
19. Kanehisa M, et al. (2014) Data, information, knowledge and principle: Back to metabolism in KEGG. *Nucleic Acids Res* 42(Database issue):D199–D205.
20. Thoden JB, Kim J, Raushel FM, Holden HM (2003) The catalytic mechanism of galactose mutarotase. *Protein Sci* 12(5):1051–1059.
21. Stamps SL, Taylor AB, Wang SC, Hackert ML, Whitman CP (2000) Mechanism of the phenylpyruvate tautomerase activity of macrophage migration inhibitory factor: Properties of the P1G, P1A, Y95F, and N97A mutants. *Biochemistry* 39(32):9671–9678.
22. McLean R, et al. (2015) Functional analyses of resurrected and contemporary enzymes illuminate an evolutionary path for the emergence of exolysis in polysaccharide lyase family 2. *J Biol Chem* 290(35):21231–21243.
23. Lindsey HA, Gallie J, Taylor S, Kerr B (2013) Evolutionary rescue from extinction is contingent on a lower rate of environmental change. *Nature* 494(7438):463–467.